The Mechanism of MICU-Dependent Gating of the Mitochondrial Ca^{2+} Uniporter

Authors: Vivek Garg[1,*], Ishan Paranjpe[1], Tiffany Unsulangi[1], Junji Suzuki[1], Lorin S. Milescu[2], and Yuriy Kirichok[1,*].

Affiliations:

[1]Department of Physiology, University of California San Francisco, San Francisco, CA, USA.

[2]Department of Biology, University of Maryland, College Park, MD, USA.

*Correspondence to: yuriy.kirichok@ucsf.edu (YK); vivek.garg@ucsf.edu (VG)

Abstract

Mitochondrial Ca^{2+} uniporter (MCU) mediates mitochondrial Ca^{2+} uptake, regulating ATP production and cell death. According to the existing paradigm, MCU is occluded at the resting cytosolic [Ca^{2+}] and only opens above an ~400 nM threshold. This Ca^{2+}-dependent gating is putatively conferred by MICUs, EF hand-containing auxiliary subunits that block/unblock the MCU pore depending on cytosolic [Ca^{2+}]. Here we provide the first direct, patch-clamp based analysis of the Ca^{2+}-dependent MCU gating and the role played by MICUs. Surprisingly, MICUs do not occlude the MCU pore, and MCU is a constitutively active channel without cytosolic [Ca^{2+}] activation threshold. Instead, MICUs potentiate MCU activity when cytosolic Ca^{2+} binds to their EF hands. MICUs cause this potentiation by increasing the probability of open state of the MCU channel.

One Sentence Summary

Auxiliary MICU subunits do not occlude the mitochondrial Ca^{2+} uniporter (MCU) but increase its activity as cytosolic Ca^{2+} is elevated.

Main Text

Mitochondrial Ca^{2+} uptake regulates ATP production, shapes intracellular Ca^{2+} transients and plays a crucial role in deciding cell fate (*1-4*). It is mediated by the mitochondrial Ca^{2+} uniporter (MCU) (*3-5*), which upon elevation of cytosolic [Ca^{2+}] ([Ca^{2+}]$_{cyto}$) allows selective Ca^{2+} permeation into the mitochondrial matrix, down the high electrochemical gradient across the IMM. All Ca^{2+} channels lose their selectivity and become permeable for Na^{+} at low [Ca^{2+}], when Ca^{2+} is removed from the pore (*6-8*). MCU also conducts Na^{+} but only when [Ca^{2+}] is decreased to low nM range, because the MCU pore has a Ca^{2+} binding site with an exceptionally high affinity ($K_d \leq 2$ nM) (*9-15*). This prevents permeation of abundant cytosolic monovalent cations even at a resting [Ca^{2+}]$_{cyto}$ of ~100 nM, and makes MCU the most selective Ca^{2+} channel known.

MCU activity must be regulated. Insufficient Ca^{2+} uptake would result in deficient ATP production, whereas excessive uptake would lead to mitochondrial Ca^{2+} overload, $\Delta\Psi$ dissipation, mitochondrial dysfunction and cell death (*16*). A few early studies suggested that MCU activity might be potentiated by cytosolic [Ca^{2+}] (*4, 17, 18*). However, the results differed significantly between labs, because MCU activity was assessed indirectly in suspensions of isolated mitochondria and critical experimental conditions could not be reliably controlled (*3, 4*). Thus, such potentiation was controversial and no clear unifying model for Ca^{2+}-dependent MCU gating was generated.

Recent molecular characterization established that MCU is a macromolecular complex (fig. S1A). Its pore is formed by the MCU subunit (*19, 20*) and the essential MCU regulator (EMRE) subunit (*21*). EF hand domain-containing auxiliary MICU1–3 subunits are tethered on the cytosolic side of the MCU/EMRE pore (*22, 23*). MICU1 interacts directly with the MCU and

EMRE, while MICU2 and MICU3 attach to the MCU complex only by heterodimerizing with MICU1 (*21, 24-26*). MICU3 is a neuronal- and embryonic-specific isoform with little expression in other tissues (*23, 27*).

The understanding of the molecular composition of the MCU complex renewed interest in the MCU gating by cytosolic Ca^{2+}. In MICU1 deficiency, when none of the MICU subunits is associated with the MCU/EMRE pore, mitochondrial Ca^{2+} ($[Ca^{2+}]_{mito}$) starts to increase at lower $[Ca^{2+}]_{cyto}$ both in cells (*24, 25, 28-31*) and isolated mitochondria (*32*). Based on these results, the term "$[Ca^{2+}]_{cyto}$ threshold for mitochondrial Ca^{2+} uptake" was coined, and it was postulated that MICU1 (in association with other MICUs) confers the $[Ca^{2+}]_{cyto}$ threshold for MCU activation (*28, 29*). Specifically, the current paradigm suggests that at resting $[Ca^{2+}]_{cyto}$, MICU1 occludes the MCU pore (*28, 33, 34*), but when $[Ca^{2+}]_{cyto}$ increases above ~400–800 nM and Ca^{2+} binds to the MICU1 EF hands, this occlusion is relieved (*24, 28, 29*) (Fig. 6A). MICU2 is proposed to facilitate this MICU1 function (*24, 25, 35*). In this model, the occlusion of MCU by MICU1/MICU2 at the resting $[Ca^{2+}]_{cyto}$ is considered well-established (tables S1 and S2), while the degree to which the occlusion is removed at elevated $[Ca^{2+}]_{cyto}$ remains controversial with different groups reporting a wide range of effects (tables S1 and S2). *MICU1*$^{-/-}$ mice show profound late embryonic and postnatal lethality (*32, 36*), while loss-of function MICU1 mutations in humans cause fatigue, lethargy, severe myopathy, developmental and learning disabilities, and progressive extrapyramidal movement disorder (*30, 37-39*).

The paradigm that MICUs occlude the MCU pore at resting cytosolic Ca^{2+} and impart $[Ca^{2+}]_{cyto}$ activation threshold on MCU has affected the field profoundly. However, it has never been demonstrated by direct measurement of Ca^{2+} currents mediated by MCU. Instead, MCU activity was inferred from the changes in $[Ca^{2+}]$ inside or outside of mitochondria, as measured

with Ca^{2+} indicators. However, such [Ca^{2+}] changes never reflect MCU activity alone but are determined by the balance between mitochondrial Ca^{2+} uptake and efflux mechanisms (*3, 4, 40*). Some of these studies (*34, 36*) used CGP37157 to inhibit the mitochondrial Ca^{2+} efflux associated with the Ca^{2+}/Na^{+} exchange mechanism, but this was clearly insufficient to eliminate all mitochondrial Ca^{2+} efflux. Indeed, if the Ca^{2+} efflux was fully eliminated, the free $[Ca^{2+}]_{mito}$ (based on the Nernst equation and assuming 100 nM $[Ca^{2+}]_{cyto}$ and $\Delta\Psi$ at -160 mV) would reach an enormous value of ~25 mM even with residual MCU activity. Other factors such as $\Delta\Psi$, the volume of mitochondrial matrix, matrix Ca^{2+} buffering with phosphates (*40*) and pH can further confound indirect assessment of MCU activity using Ca^{2+} indicators.

The numerous pitfalls associated with indirect assessment of MCU activity make direct measurements of MCU currents (*9, 10, 41*) necessary for understanding of MCU regulation and the role of MICU subunits. However, such direct measurements have been considered extremely challenging, especially in the context of structure–function studies of the MCU complex, which require assessment of numerous knockout and mutant models. There have been a few attempts to characterize MICU1-dependent regulation of MCU using direct electrophysiology, but the scope of electrophysiological experiments in these few studies was very limited, and MICU1 function was assessed only at high $[Ca^{2+}]_{cyto}$ (*42-44*). These incomplete electrophysiological studies generated very diverse results ranging from inhibition to no effect of MICU1 on the MCU activity, and thus no clarity was achieved (table S1). One electrophysiological study tried to assess the effects of MICU1 and MICU2 at both low and high $[Ca^{2+}]_{cyto}$ (table S1) (*25*). Unfortunately, in this study a recombinant MCU subunit was reconstituted in planar lipid bilayers in the absence of EMRE, the subunit essential for both a functional MCU channel and the association of MICU1/MICU2 with the MCU pore (*25*). The observed channel conducted

Na^+ even at μM [Ca^{2+}] and failed to replicate the exceptionally high MCU selectivity for Ca^{2+}. Thus, the channel activity observed in this EMRE-less system was artifactual.

Therefore, to facilitate a rigorous and systematic insight into the function of MICU1–3, as well as other subunits of the MCU complex, we developed a heterologous expression system for direct patch-clamp analysis of the MCU complex in the native IMM. Using this system, we demonstrate that MICUs do not occlude the MCU pore. An accompanying paper (*Zhuo et al., companion manuscript*), reporting the first complete structure of the human MCU complex, also shows that MICU1/MICU2 are tethered to the periphery of the MCU-EMRE pore and do not occlude the pore. We next demonstrate that the actual function of the MICU subunits is to potentiate MCU activity when their EF hands bind cytosolic Ca^{2+}. Thus, MCU has no intrinsic $[Ca^{2+}]_{cyto}$ activation threshold. It is a constitutively active channel that is potentiated by $[Ca^{2+}]_{cyto}$ via the MICU subunits.

Results

System for direct structure–function analysis of MCU

Two factors are crucial to the success of the whole-IMM patch-clamp: the size of individual mitoplasts (vesicles of the whole native IMM) and the IMM stability during the electrophysiological experiments. Therefore, we tested various cell lines for the best possible optimization of these two factors. Eventually, we selected a *Drp1*$^{-/-}$ MEF cell line (*45*), in which mitochondria form long tubular networks and provide a significantly higher proportion of large isolated mitoplasts that are also remarkably resilient during the whole-IMM electrophysiological experiments. We confirmed that this cell line expresses all principal subunits of the MCU complex (fig. S2A-D). We next generated gene knockouts for all principal subunits of the MCU

complex (MCU, EMRE and MICU1–3) using CRISPR-Cas9 in the background of *Drp1*$^{-/-}$ MEFs (fig. S1). All knockout cell lines lacked protein expression of the respective subunit (fig. S2A-C).

To explore the cytosolic/mitochondrial Ca^{2+} phenotypes in these MCU complex knockout cell lines, we induced slow elevation of $[Ca^{2+}]_{cyto}$ using the SERCA inhibitor thapsigargin (Tg) and observed an associated increase in $[Ca^{2+}]_{mito}$ (fig. S2E-J). $[Ca^{2+}]_{cyto}$ was measured using Fura-2 while the mitochondrial Ca^{2+} changes were measured using a genetically-encoded Ca^{2+} indicator *Cepia* (*46*) targeted to mitochondria. $[Ca^{2+}]_{cyto}$ under resting conditions was maintained ~75 nM in all cell lines (fig. S2K) and peaked in the range of 400–1000 nM upon addition of Tg (fig. S2L). In cells with the *WT* MCU complex, the $[Ca^{2+}]_{cyto}$ increase was followed, after a short delay, by $[Ca^{2+}]_{mito}$ elevation (fig. S2E). However, as expected, in *MCU*$^{-/-}$ or *EMRE*$^{-/-}$ cell lines that have no functional MCU complex (*19-21*), no significant $[Ca^{2+}]_{mito}$ elevation was observed (fig. S2F and G). In MICU1–3-deficient cells, the $[Ca^{2+}]_{cyto}$ threshold for elevation of $[Ca^{2+}]_{mito}$ was altered as compared to that in cells with the *WT* MCU complex (fig. S2H-J, and M). In *MICU1*$^{-/-}$ cells, the threshold was drastically decreased (fig. S2H and M), and a significant but less profound decrease was also observed in *MICU2*$^{-/-}$ cells (fig. S2I and M). However, *MICU3*$^{-/-}$ cells had an increased threshold (fig. S2J and M). Thus, in our cell system, we observed the same $[Ca^{2+}]_{mito}$ phenotypes associated with knockout of individual MCU complex subunits as reported previously (*24, 25, 28, 29, 34*)**.**

We next explored how knockouts for various MCU complex subunits affect MCU currents. Importantly, the MCU complex was intact in isolated whole-IMM vesicles (mitoplasts) used in our patch-clamp experiments, and its composition was the same as in intact mitochondria based on MCU-FLAG co-immunoprecipitation experiments (fig. S4A). Mitoplasts isolated from cells with the *WT* MCU complex had a robust whole-IMM Ca^{2+} current (I_{Ca}). The voltage step

from 0 to -160 mV, followed by a voltage ramp to +80 mV, elicited an inwardly rectifying I_{Ca} that gradually increased as $[Ca^{2+}]_{cyto}$ (bath solution) was elevated (Fig. 1A, *left panel*, and fig. S3A and B). As expected, in a Ca^{2+}-free bath solution (control), we only observed an outward Na^+ current (I_{Na}, black trace) via MCU, because the pipette solution contained Na^+ (Fig. 1A, *left panel*, and fig. S3A and B).

Mitoplasts isolated from *MCU*$^{-/-}$ and *EMRE*$^{-/-}$ lines had no inward I_{Ca} or outward I_{Na}, confirming the essential role of these two subunits for the functional MCU complex (*21, 47, 48*) (Fig. 1A and C). Importantly, even millimolar $[Ca^{2+}]_{cyto}$ induced no I_{Ca} in *MCU*$^{-/-}$ and *EMRE*$^{-/-}$, demonstrating that MCU is the only electrogenic mechanism for mitochondrial Ca^{2+} uptake. Heterologous expression of MCU or EMRE in their corresponding knockout cell lines (fig. S4B and C) resulted in restoration of the inward I_{Ca} and outward I_{Na} (Fig. 1B and C).

Thus, we have identified a system that has robust MCU currents, can be used for heterologous expression of recombinant MCU complex subunits, and significantly improves throughput of whole-IMM patch-clamp recording.

MICUs are Ca^{2+}-dependent MCU potentiators

In contrast to *MCU*$^{-/-}$ and *EMRE*$^{-/-}$, none of the MICU knockouts (MICU1–3) showed loss of I_{Ca} or I_{Na} (Fig. 1D), demonstrating that these subunits are not absolutely required for a functional MCU channel. However, among all MICU knockouts, loss of MICU1 resulted in a marked reduction (~50%) of I_{Ca} in both micromolar and millimolar ranges of $[Ca^{2+}]_{cyto}$ (Fig. 1D and E, and fig. S5). The same reduction was observed when I_{Ca} was measured at both -160 mV (Fig. 1E) and -80 mV (fig. S5C). We next focused on understanding the mechanism by which MICU1 regulates MCU function.

As was suggested previously, MICU1 tethers other MICU subunits to the MCU/EMRE pore (*21, 24-26*). The accompanying paper reporting the structure of the complete human MCU complex confirms that the MICU1/MICU2 dimer is tethered to the MCU/EMRE pore specifically via interactions between MICU1 and EMRE (*Zhuo et al., accompanying manuscript*). Thus, in *MICU1*$^{-/-}$ none of the MICU subunits are associated with the MCU complex. The levels of MCU and MCUb (MCU paralog with no Ca^{2+} transport activity and putative dominant-negative effect on the MCU function) subunits (*49*) were not affected in *MICU1*$^{-/-}$, while EMRE expression was significantly reduced (fig. S6A-D), as was also shown previously (*32*). The lower EMRE expression in *MICU1*$^{-/-}$ was not a limiting factor for I_{Ca}, because EMRE overexpression in *MICU1*$^{-/-}$ cells did not rescue the I_{Ca} reduction (fig. S6D-F). Therefore, the I_{Ca} reduction in *MICU1*$^{-/-}$ was caused by the lack of MICU1 (and other MICU proteins) in the MCU complex. Because I_{Ca} was recorded at $[Ca^{2+}]_{cyto} \geq 10$ μM, when the EF hands of MICU subunits (K_d ~600 nM) (*50*) are occupied by Ca^{2+}, we conclude that in the Ca^{2+}-bound state MICUs potentiate the MCU current.

We next studied how MICUs affect the MCU current when Ca^{2+} is not bound to their EF hands. Because this requires $[Ca^{2+}]_{cyto}$ <60 nM (10-fold less than *Kd*) and I_{Ca} cannot be measured reliably under these conditions, we used Na^+ as the permeating ion. A robust I_{Na} via MCU was observed when Ca^{2+} was eliminated on the cytosolic face of the IMM with Ca^{2+} chelators (Fig. 2A, *left panel*). As expected, I_{Na} completely disappeared in *MCU*$^{-/-}$ and *EMRE*$^{-/-}$ (Fig. 2A and B). Interestingly, in a striking contrast to I_{Ca}, I_{Na} was not reduced in *MICU1*$^{-/-}$, (Fig. 2C-E, also see Fig. 1D and E). The very presence of a robust I_{Na}, and the fact that it is not altered in *MICU1*$^{-/-}$, argues strongly against the currently accepted paradigm (*33, 34*) in which the MCU/EMRE pore is occluded by MICUs when their EF hands are not occupied by Ca^{2+} (Fig. 6A). In the absence of

cytosolic Ca^{2+}, a robust I_{Na} via MCU was also previously recorded in mitoplasts isolated from COS-7 cells, mouse heart and skeletal muscle (*9, 10*). Nanomolar concentrations of MCU inhibitor ruthenium red (RuR) completely block this I_{Na} (*9, 10*). In the absence of divalent cations, a RuR-sensitive, Na^+-selective MCU-dependent uniport was also reported in intact isolated mitochondria (*51, 52*). Thus, the MCU/EMRE pore is not occluded by MICU proteins when Ca^{2+} is not bound to their EF hands. Moreover, the similarity of I_{Na} amplitudes in *WT* and *MICU1*$^{-/-}$ (Fig. 2C-E) suggests that in their Ca^{2+}-free state MICUs do not affect ion permeation through the MCU/EMRE pore at all. The accompanying structural paper describing the human MCU complex also demonstrates that MICU1/MICU2 do not occlude the pore entrance. Moreover, the profile of the MCU pore is the same, with or without MICU1/MICU2 attached (*Zhuo et al., companion manuscript*).

The *MICU1*$^{-/-}$ phenotypes of I_{Na} (no change) and I_{Ca} (reduction) suggest that the only function of MICUs is potentiation of the MCU complex activity when their EF hands are occupied by Ca^{2+}. To further examine this phenotype, we studied how the ratio of I_{Ca} to I_{Na}, as measured in the same mitoplast, is affected by *MICU1*$^{-/-}$. Such I_{Ca}/I_{Na} ratio depends only on the functional properties of the MCU complex, and, in contrast to I_{Ca} and I_{Na} amplitudes, is independent of the number of MCU complexes in a mitoplast. Thus, an alteration of the I_{Ca}/I_{Na} ratio in *MICU1*$^{-/-}$ can be directly attributed to altered functional properties of the MCU complex, and would not depend on any associated changes in MCU/EMRE expression affecting the number of MCU complexes.

The I_{Ca}/I_{Na} ratio was dramatically reduced in *MICU1*$^{-/-}$ mitoplasts (Fig. 2F), which means that the loss of MICUs is directly responsible for the reduction of I_{Ca} as compared to I_{Na}. The loss of MICUs can cause such reduction in the I_{Ca}/I_{Na} ratio by either altering the channel gating or

affecting the relative affinities for Ca^{2+} and Na^{+} binding in the selectivity filter. The reduction in I_{Ca}/I_{Na} ratio in *MICU1*$^{-/-}$ could not be explained by altered relative affinities for Ca^{2+} and Na^{+} binding in the selectivity filter, because I_{Na} was inhibited to the same extent by 2 nM $[Ca^{2+}]_{cyto}$ in both *WT* and *MICU1*$^{-/-}$ mitoplasts (Fig. 2G and H). Thus, a reduced I_{Ca}/I_{Na} ratio in *MICU1*$^{-/-}$ is caused by a disrupted MICU-dependent gating mechanism. This gating mechanism potentiates MCU currents in a Ca^{2+}-dependent fashion.

The above experiments were all performed in cell lines with disrupted *Drp1*. However, *Drp1* is not a part of the MCU complex, and therefore *Drp1* loss is not expected to affect MCU currents as measured directly with patch-clamp electrophysiology. Indeed, in our experiments *Drp1* knockout did not affect the amplitudes of I_{Ca} or I_{Na} mediated by the MCU complex (fig. S7A and B). However, we still confirmed that the observed *MICU1*$^{-/-}$ current phenotypes were the same, irrespective of the *Drp1* background. Similar to MICU1 knockout in *Drp1*$^{-/-}$ MEFs, MICU1 knockout in *Drp1*$^{+/+}$ MEFs did not affect I_{Na} while markedly reduced I_{Ca} (fig. S7C-E). Additionally, *MICU1*$^{-/-}$ reduced the I_{Ca}/I_{Na} ratio, as measured in the same mitoplast, to the similar extent in *Drp1*$^{+/+}$ MEFs (fig. S7F). Thus, as expected, *Drp1* presence or absence does not affect currents mediated by the MCU complex or the *MICU1*$^{-/-}$ phenotypes.

To conclude, MICU subunits do not occlude the MCU/EMRE pore or impart a $[Ca^{2+}]_{cyto}$ activation threshold on the MCU complex. Instead, MCU is a constitutively active channel, and the actual function of MICU subunits is to potentiate MCU currents as $[Ca^{2+}]_{cyto}$ is elevated.

Role of EF hands of MICUs in I_{Ca} potentiation

To confirm that Ca^{2+} binding to the EF hands of MICUs is responsible for the Ca^{2+}-dependent potentiation of MCU, we recombinantly expressed MICU1–3 or MICU1–3 with

mutated EF hands (mut-EF-MICU, to disable Ca^{2+} binding (*24*)) in their respective knockout cell lines and examined the changes in I_{Ca} (Fig. 3A).

In *MICU1*$^{-/-}$, expression of MICU1 was able to restore I_{Ca} to the *WT* level, but mut-EF-MICU1 expression failed to do so (Fig. 3B). Expression levels of both the recombinant MICU1 and mut-EF-MICU1 were significantly higher as compared to MICU1 expression in the cells with *WT* MCU complex (Fig. 3A). This confirms our hypothesis that Ca^{2+} binding to the EF hands of MICU1 is indispensable for I_{Ca} potentiation.

In *MICU2*$^{-/-}$, I_{Ca} was not significantly affected (Fig. 3C, and 1D and E), because the loss of MICU2 appeared to be compensated with increased MICU1 expression and replacement of MICU1/MICU2 heterodimer with MICU1/MICU1 homodimer (fig. S8A-C). Therefore, overexpression of recombinant MICU2 in *MICU2*$^{-/-}$ and preferential conversion of MICU1/MICU1 homodimers back into MICU1/MICU2 heterodimers also did not alter the I_{Ca} amplitude (Fig. 3C). In contrast, mut-EF-MICU2 overexpression displaced MICU1 from MICU1/MICU1 homodimers in favor of MICU1/mut-EF-MICU2 heterodimer, leading to a dominant-negative effect and a significant decrease in MICU-dependent I_{Ca} potentiation (Fig. 3C). These functional data, combined with biochemical evidence for MICU1/MICU2 heterodimers (*25, 53, 54*) (also see the companion manuscript by *Zhou et al.*), suggest that MICU2, along with MICU1, is responsible for allosteric potentiation of MCU upon binding of cytosolic Ca^{2+} to their EF hands.

The effect of *MICU1*$^{-/-}$ on I_{Ca} was more profound as compared to that of *MICU2*$^{-/-}$ (Fig. 1D and E), because MICU1 could compensate for MICU2. However, the reverse compensation was impossible, because only MICU1 tethers the MICU1/MICU2 heterodimer to the MCU/EMRE pore (*Zhuo et al., companion manuscript*). The composition of MICU dimers can

also be affected by MICU3 that similar to MICU2 was proposed to interact and form heterodimers with MICU1 (*27*). However, in our experiments, we did not observe robust current phenotypes associated with MICU3. Specifically, I_{Ca} was not affected in *MICU3*$^{-/-}$ mitoplasts, and overexpression of recombinant MICU3 or mut-EF-MICU3 in *MICU3*$^{-/-}$ also had no effect on I_{Ca} (Fig. 3D). It has been suggested that MICU3 is a minor protein as compared to MICU1 and 2 in the majority of tissues and cell lines assessed (*27*). Although in our system the amount of MICU3 mRNA appeared to be comparable with that of other MICU subunits (fig. S2D), and the MICU3 protein was expressed (Fig. 3A *right panel*, and fig. S2C), the relative abundance of MICU3 vs other MICUs is not clear. Moreover, in contrast to MICU1, MICU3 is not upregulated in *MICU2*$^{-/-}$ cells (fig. S8B), and thus, MICU3 expression does not appear to be linked to the level of MICU2. Therefore, although MICU3 could in principle support the Ca^{2+}-dependent potentiation of MCU by forming dimers with MICU1 (*27*), the exact role of MICU3 and its interaction with other MCU complex subunits remains to be established.

Ca^{2+} binding to the EF hands of MICU subunits and a subsequent conformational change that potentiates the MCU complex activity require a finite time and may delay I_{Ca} activation/deactivation in response to changes in $[Ca^{2+}]_{cyto}$. Such delayed I_{Ca} kinetics can profoundly affect $[Ca^{2+}]_{mito}$, because in situ MCU takes up Ca^{2+} from Ca^{2+} microdomains (*55*) that exist in the cytosol only for a few milliseconds (*56*). Therefore, we examined I_{Ca} activation and deactivation kinetics in response to rapid changes in $[Ca^{2+}]_{cyto}$ and tested whether they depend on MICUs. I_{Ca} activation upon rapid elevation of $[Ca^{2+}]_{cyto}$ from virtually Ca^{2+}-free to 1 mM was immediate, with kinetics comparable to the rate of solution exchange (τ ~0.4 ms) achieved by our piezoelectric fast application system (Fig. 3E). Importantly, the kinetics of the I_{Ca} rapid response was not altered in *MICU1*$^{-/-}$ (Fig. 3E and F). The deactivation kinetics was

similarly fast and not dependent on MICU1 (Fig. 3E and F). The result of these experiments correspond to the previous observation that EF hands of calmodulin bind Ca^{2+} with a μs time constant (*57*). The conclusion from these experiments is that the kinetics of Ca^{2+} binding to the MICU's EF hands, and the resultant conformational change in the MCU complex, are extremely fast, and thus MICU-dependent potentiation of the MCU activity should occur instantaneously upon elevation of the $[Ca^{2+}]_{cyto}$. This is perhaps true even within Ca^{2+} microdomains, but it has to be taken into account that in our experiments we used somewhat higher $[Ca^{2+}]_{cyto}$ (1 mM) as compared to the maximal $[Ca^{2+}]_{cyto}$ achieved in the microdomains (100 μM).

A phenomenon of Ca^{2+}-induced mitochondrial Ca^{2+} release (mCICR) by which mitochondria release Ca^{2+} into cytosol in response to elevations of $[Ca^{2+}]_{cyto}$ has been observed (*4, 58, 59*). mCICR required mitochondrial depolarization and was proposed to be mediated by MCU (*60, 61*) and/or the permeability transition pore (PTP) (*58, 59*). Therefore, we tested whether MCU can mediate Ca^{2+}-dependent Ca^{2+} efflux at depolarized membrane voltages and whether such efflux is dependent on MICUs. We measured outward I_{Ca} at positive voltages with 2 mM $[Ca^{2+}]_{mito}$ (the pipette solution), as $[Ca^{2+}]_{cyto}$ was gradually elevated from virtual zero to 1 mM. Remarkably, such $[Ca^{2+}]_{cyto}$ elevation failed to induce any outward I_{Ca}. However, as expected, it caused a robust inward I_{Ca} (Fig. 3G). This experiment also demonstrates, as was also suggested previously (*9*), that MCU has a strong inward rectification (unidirectional Ca^{2+} permeation into the matrix). This strong inward rectification of MCU under various $[Ca^{2+}]_{cyto}$ remained unaltered in *MICU1*$^{-/-}$ (Fig. 3G). Thus, MCU has a strong preference for conducting Ca^{2+} into mitochondria and is unlikely to mediate Ca^{2+} release via mCICR.

It has also been suggested that MCU is regulated by matrix $[Ca^{2+}]$ (*62*). Specifically, I_{Ca} was shown to be profoundly reduced at $[Ca^{2+}]_{mito}$ ~400 nM, as compared to that at both lower

(Ca^{2+}-free) and higher (high μM) $[Ca^{2+}]_{mito}$ (*62*). The authors also proposed that the reduction of the MCU current at $[Ca^{2+}]_{mito}$ ~400 nM is MICU1-dependent. However, in contrast to this previous observation, in our experiments I_{Ca} amplitude remained unaltered when $[Ca^{2+}]_{mito}$ was set at Ca^{2+}-free, 400 nM, or 400 μM (fig. S9). Thus, the MCU complex is not regulated by matrix Ca^{2+}, and MICUs only impart the regulation of the MCU complex by cytosolic Ca^{2+}. It should also be mentioned that the authors proposed a membrane topology of EMRE (*62*) that is reverse to that determined in the recent biochemical and structural studies (*14, 26*) (see also the accompanying manuscript by *Zhuo et al.*).

Taken together, these data indicate that MICU proteins allosterically potentiate MCU-mediated Ca^{2+} influx when cytosolic Ca^{2+} binds to their EF hands.

MICUs increase the open probability of MCU

To investigate the mechanism by which Ca^{2+}-bound MICU proteins potentiate I_{Ca}, we examined the activity of single MCU channels in inside-out (matrix-side out) IMM patches. Because the unitary Ca^{2+} current (i_{Ca}, current via a single MCU channel) is very small (<1 pA), it must be recorded at high $[Ca^{2+}]$=105 mM to improve resolution (*9*). At this $[Ca^{2+}]$, EF hands of MICU subunits are fully saturated with Ca^{2+}.

MCU exhibits multiple levels of single channel conductance. These subconductances can be observed at all tested voltages (-40, -80, and -120 mV), but their resolution improves markedly as transmembrane voltage becomes more negative. At -120 mV, in addition to what appears to be a fully open i_{Ca}, subconductances at ~0.8 and ~0.6 of the amplitude of the fully open i_{Ca} can be easily detected (Fig. 4A and C). Because similar amplitude levels were observed in all the patches, we conclude that these events represent genuine subconductances in the MCU

channel.

There was no difference in the single channel amplitude between control and *MICU1*$^{-/-}$ mitoplasts (Fig. 4A-C). However, we found that the single-channel open probability (*P*o) was significantly decreased ~2–3 fold in *MICU1*$^{-/-}$ versus *WT* mitoplasts, depending on the transmembrane voltage (Fig. 4A, B, D and fig. S10A-C). As a result, the time-averaged current contributed by a single MCU channel differs significantly between control and *MICU1*$^{-/-}$ mitoplasts (Fig. 4E), thus mirroring and explaining the effect of MICU1 knockout on the amplitude of the whole-mitoplast I_{Ca} (Fig. 1E).

These results demonstrate that the potentiating effect of MICU proteins on the MCU/EMRE pore is not associated with an increased single-channel conductance. Rather, when their EF hands bind Ca^{2+}, MICUs increase MCU currents by causing an increase in the open probability of the MCU/EMRE pore.

MICU1 does not affect the Mn^{2+} vs Ca^{2+} permeability of MCU

While Mn^{2+} is essential for the proper function of several mitochondrial enzymes, its excessive accumulation inhibits oxidative phosphorylation and causes toxicity (*63*). MCU appears to be the primary pathway for Mn^{2+} entry into mitochondria (*4*). Recently, it has been suggested that MICU1 is responsible for the relatively low permeability of MCU for Mn^{2+} as compared to Ca^{2+}, and MICU1 deficiency or loss-of-function MICU1 mutations in patients can lead to excessive mitochondrial Mn^{2+} accumulation and cellular toxicity (*42, 64*). These observations were explained within the paradigm in which MICU1 occludes the MCU/EMRE pore. It was postulated that Mn^{2+} binds to MICU1 EF hands but, in contrast to Ca^{2+}, cannot induce the MICU1 conformation change necessary to unblock the MCU pore. Thus, MICU1

prevents Mn^{2+} permeation via MCU and ensures selective Ca^{2+} permeation (*42, 64*).

We recorded the inward Mn^{2+} current (I_{Mn}) in the presence of 5 mM $[Mn^{2+}]_{cyto}$. I_{Mn} disappeared in *MCU*$^{-/-}$ and *EMRE*$^{-/-}$, confirming that it was solely mediated by MCU (Fig. 5A-D). As was also shown previously (*9*), I_{Mn} was indeed significantly smaller (~7-fold) than I_{Ca} at 5 mM $[Mn^{2+}]_{cyto}$ and 5 mM $[Ca^{2+}]_{cyto}$, respectively (Fig. 5E). However, we also observed that I_{Mn} and I_{Ca} were reduced to a similar extent in *MICU1*$^{-/-}$ (Fig. 5F-H). This result was in a striking contrast to the current MICU1-based model for Mn^{2+} vs Ca^{2+} selectivity of MCU (*42, 64*), under which I_{Mn} would be increased but I_{Ca} not affected under our experimental conditions. Moreover, even the ratio between I_{Mn} and I_{Ca} calculated from the same mitoplast (I_{Mn}/I_{Ca}) was not affected in *MICU1*$^{-/-}$ (Fig. 5I), although it is expected to be decreased as per the MICU1-based model for Mn^{2+} vs Ca^{2+} selectivity of MCU (*42, 64*). Finally, Mn^{2+} inhibited I_{Ca} to the same extent in *WT* and *MICU1*$^{-/-}$ mitoplasts (Fig. 5F and J), indicating that Ca^{2+} and Mn^{2+} are likely to compete in the selectivity filter of the MCU/EMRE pore.

Thus, the I_{Ca} and I_{Mn} phenotypes of *MICU1*$^{-/-}$ are the same, and MICU1 does not determine the preference of MCU for Ca^{2+} over Mn^{2+}. Permeation of both Ca^{2+} and Mn^{2+} is enhanced, rather than inhibited by MICU1. Instead of MICU1, the selectivity of the MCU complex for Ca^{2+} over Mn^{2+} (and for any other ion) should be determined by the selectivity filter located in the pore (*11-13, 15*), exactly as in other ion channels. Thus, the properties of Mn^{2+} permeation via MCU cannot be explained within the paradigm in which MICUs occlude the MCU/EMRE pore, nor it can be used to validate it.

Discussion

In summary, the direct patch-clamp analysis presented here argues for a significant

revision of the current paradigm for the gating of the MCU complex, its control by $[Ca^{2+}]_{cyto}$, and the role played by MICU subunits (Fig. 6).

In contrast to the existing model, we demonstrated that at low $[Ca^{2+}]_{cyto}$, when EF hands of MICU subunits are Ca^{2+}-free, the MCU/EMRE pore is not occluded by MICUs and conducts robust Na^{+} current regardless of MICU's presence. Thus, the MCU complex is a constitutively active channel. We further demonstrated that the real function of MICU subunits is to potentiate the activity of the MCU complex as cytosolic Ca^{2+} is elevated and binds to MICU's EF hands (Fig. 6B). MICU subunits potentiate MCU activity by increasing the open state probability of the MCU/EMRE pore. MICUs are likely to achieve this effect by interacting with EMRE that is predicted to control the gating of the MCU/EMRE pore (*14*). The structure of the complete MCU complex presented in the accompanying paper clarifies this mechanism further and suggests that MICU1/MICU2 dimers connect (at the cytosolic side) EMREs of two different MCU/EMRE pores and could control MCU gating by pulling on these EMREs (*Zhuo et al., accompanying manuscript*).

MICU1/MICU2 dimer binds cytosolic Ca^{2+} with K_d ~600 nM (*50*). To understand the Ca^{2+}-dependent function of the MICU1/MICU2 dimer, the effects of MICUs on the MCU/EMRE pore must be studied at the two extremes of the EF-hand Ca^{2+} titration range – when all MICUs are essentially Ca^{2+}-free and when they are fully occupied by Ca^{2+}. This can be achieved by measuring the two types of currents via the MCU complex - I_{Na} and $I_{Ca.}$

As we demonstrated previously (*9, 10*) and also elaborate in this work, the MCU complex can conduct both Na^{+} and Ca^{2+}. This is because Ca^{2+} and Na^{+} have very similar radii and both can bind to and permeate through the narrowest Ca^{2+} binding site in the MCU selectivity filter, similar to other Ca^{2+} channels (*6, 11-13*). I_{Na} and I_{Ca} have been instrumental in understanding the

MCU channel and its exceptionally high Ca^{2+} selectivity (*9*, *10*). I_{Na} is measurable only when $[Ca^{2+}]_{cyto} \leq 2$ nM (Fig. 2G), while I_{Ca} can only be measured at $[Ca^{2+}]_{cyto} \geq 10$ µM (Fig. 1D). In between 2 nM and 10 µM, lies a $[Ca^{2+}]_{cyto}$ range where MCU currents are extremely small and cannot be measured reliably. Such "no-current" range is not a unique property of MCU, but is a characteristic property of all Ca^{2+}-selective channels and is explained by the anomalous mole-fraction effect, a phenomenon of binding and competition between two different ions (Na^{+} and Ca^{2+}) in the selectivity filter (*65*). However, by measuring I_{Na} and I_{Ca}, the patch-clamp electrophysiology can reliably establish the effect of MICUs on the MCU/EMRE pore at the two extremes of the EF-hand Ca^{2+} titration range – when all EF hands are either in the Ca^{2+}-free state or in the Ca^{2+}-occupied state. It is important to understand that such direct measurement of I_{Na} and I_{Ca} is the only reliable way to assess the function of MICU subunits within the MCU complex.

It is tempting to assume that optical methods can assess the MCU complex activity and the MICU function continuously over a wide $[Ca^{2+}]_{cyto}$ range, starting from high nM. This perceived "high sensitivity" of optical methods is achieved by integration of the net mitochondrial Ca^{2+} influx (even if it is very slow) over a period of time, resulting in a measurable $[Ca^{2+}]_{mito}$ change. However, it must be realized that the optical methods do not measure MCU activity directly or in isolation from other Ca^{2+} transport mechanisms, and do not permit adequate control over the experimental conditions. When $[Ca^{2+}]_{cyto}$ is in the high nM range (around the resting levels), the MCU-mediated Ca^{2+} uptake is very slow and exists in an equilibrium with the mitochondrial Ca^{2+} efflux mechanisms (*40*). Thus, any measured changes in $[Ca^{2+}]_{mito}$ cannot be assigned to MCU exclusively. When $[Ca^{2+}]_{cyto}$ is elevated into the µM range, the MCU activity becomes high and overwhelms not only the Ca^{2+} efflux machinery but also the

electron transport chain, resulting in a decreased driving force for Ca^{2+} and underestimation of the MCU activity (*3, 4*). Because of all these technical limitations, measuring the effect of MICU knockouts on I_{Na} at nM $[Ca^{2+}]_{cyto}$ and on I_{Ca} at µM $[Ca^{2+}]_{cyto}$ with direct patch-clamp electrophysiology is the only way to reliably study the MICU function.

Here we demonstrate that the MCU complex is constitutively active and has no intrinsic $[Ca^{2+}]_{cyto}$ threshold. A recent report also suggested no apparent $[Ca^{2+}]_{cyto}$ threshold for MCU in heart and skeletal muscle (*66*). Thus, the $[Ca^{2+}]_{cyto}$ threshold for elevation of $[Ca^{2+}]_{mito}$ is simply determined by the equilibrium between the MCU-dependent Ca^{2+} uptake and the mitochondrial Ca^{2+} efflux mechanisms. Such a simple equilibrium-based $[Ca^{2+}]_{cyto}$ threshold for $[Ca^{2+}]_{mito}$ elevation was proposed previously and was termed the "set point" (*40*).

Assuming that the K_d for Ca^{2+} binding to MICU EF hands is ~600 nM (*50*), MICUs would start potentiating the MCU complex activity already in the high nanomolar range of $[Ca^{2+}]_{cyto}$, around the resting levels. Thus, MICUs should help MCU to overcome the mitochondrial Ca^{2+} efflux machinery and decrease the set point.

It is therefore paradoxical that the optical studies report not an increase but a decrease in "threshold" for mitochondrial Ca^{2+} uptake in *MICU1*$^{-/-}$. However, it simply illustrates that the results of the optical experiments should be interpreted with a caution not only at the level of MCU but also at the level of the whole organelle. The set point for mitochondrial Ca^{2+} accumulation is affected not only by the MCU-mediated uptake but also by mitochondrial Ca^{2+} efflux and numerous other factors such as $\Delta\psi$, matrix pH, permeability of the outer mitochondrial membrane, and mitochondria-ER interface, to mention the most obvious. These factors can also change and overcompensate for the reduced MCU activity in *MICU1*$^{-/-}$, resulting in a decreased set point. In contrast to the *MICU1*$^{-/-}$, such overcompensation, however, cannot

correct the phenotype of MCU and EMRE knockouts because the mitochondrial Ca^{2+} uptake is completely eliminated. To further illustrate these points, in species other than mammals, where the compensatory mechanisms induced by MICU1 knockout may be different, the $[Ca^{2+}]_{cyto}$ "threshold" for $[Ca^{2+}]_{mito}$ elevation is affected in a different way, although the composition of the MCU complex (including EMRE and MICU1) is similar to mammals. Specifically, in *Trypanosoma cruzi*, MICU1 knockout causes an increase in the Ca^{2+} uptake "threshold" and a marked decrease in Ca^{2+} uptake capacity at all $[Ca^{2+}]_{cyto}$ (*67*). The possibility that MICU proteins have other functions (*68*) beyond being a part of the MCU complex can further complicate the interpretation of the *MICU1*$^{-/-}$ phenotype as assessed by optical methods. In *Drosophila*, a lethal phenotype of MICU1 knockout was not rescued when combined with either MCU or EMRE knockouts (the MCU and EMRE knockouts themselves had mild phenotypes), suggesting functions for MICU proteins beyond the MCU complex (*68*). Thus, the results obtained with optical methods must be interpreted with due consideration to direct electrophysiological and structural data on the MCU complex. Otherwise, not only the properties of the MCU complex, but also mitochondrial Ca^{2+} homeostasis in general will be misunderstood.

In summary, we demonstrate that MICUs are Ca^{2+}-dependent MCU potentiators. They are likely to exert their potentiating effect over a range of $[Ca^{2+}]_{cyto}$ from resting to high micromolar. By doing so, MICUs can control both the $[Ca^{2+}]_{cyto}$ set point for $[Ca^{2+}]_{mito}$ elevation and the maximum $[Ca^{2+}]_{mito}$ reached during intracellular Ca^{2+} signaling. Importantly, the potentiation of MCU by MICUs could help to reduce the number of MCU channels required for adequate Ca^{2+}-dependent stimulation of mitochondrial ATP production. Without MICUs, the number of MCU channels per mitochondrion would have to be ~2 times higher, which would also increase futile Ca^{2+} cycling at resting $[Ca^{2+}]_{cyto}$.

REFERENCES AND NOTES

1. B. Glancy, R. S. Balaban, Role of mitochondrial Ca2+ in the regulation of cellular energetics. *Biochemistry* **51**, 2959-2973 (2012).

2. M. J. Berridge, M. D. Bootman, H. L. Roderick, Calcium signalling: dynamics, homeostasis and remodelling. *Nature reviews* **4**, 517-529 (2003).

3. P. Bernardi, Mitochondrial transport of cations: channels, exchangers, and permeability transition. *Physiol Rev* **79**, 1127-1155 (1999).

4. T. E. Gunter, D. R. Pfeiffer, Mechanisms by which mitochondria transport calcium. *Am J Physiol* **258**, C755-786 (1990).

5. H. F. Deluca, G. W. Engstrom, Calcium uptake by rat kidney mitochondria. *Proc Natl Acad Sci U S A* **47**, 1744-1750 (1961).

6. L. Tang *et al.*, Structural basis for Ca2+ selectivity of a voltage-gated calcium channel. *Nature* **505**, 56-61 (2014).

7. P. Hess, J. B. Lansman, R. W. Tsien, Calcium channel selectivity for divalent and monovalent cations. Voltage and concentration dependence of single channel current in ventricular heart cells. *J Gen Physiol* **88**, 293-319 (1986).

8. P. Hess, R. W. Tsien, Mechanism of ion permeation through calcium channels. *Nature* **309**, 453-456 (1984).

9. Y. Kirichok, G. Krapivinsky, D. E. Clapham, The mitochondrial calcium uniporter is a highly selective ion channel. *Nature* **427**, 360-364 (2004).

10. F. Fieni, S. B. Lee, Y. N. Jan, Y. Kirichok, Activity of the mitochondrial calcium uniporter varies greatly between tissues. *Nat Commun* **3**, 1317 (2012).

11. N. X. Nguyen *et al.*, Cryo-EM structure of a fungal mitochondrial calcium uniporter. *Nature* **559**, 570-574 (2018).

12. C. Fan *et al.*, X-ray and cryo-EM structures of the mitochondrial calcium uniporter. *Nature* **559**, 575-579 (2018).

13. R. Baradaran, C. Wang, A. F. Siliciano, S. B. Long, Cryo-EM structures of fungal and metazoan mitochondrial calcium uniporters. *Nature* **559**, 580-584 (2018).

14. Y. Wang *et al.*, Structural Mechanism of EMRE-Dependent Gating of the Human Mitochondrial Calcium Uniporter. *Cell* **177**, 1252-1261 e1213 (2019).

15. J. Yoo *et al.*, Cryo-EM structure of a mitochondrial calcium uniporter. *Science* **361**, 506-511 (2018).

16. P. Bernardi, A. Rasola, Calcium and cell death: the mitochondrial connection. *Subcell Biochem* **45**, 481-506 (2007).

17. H. Kroner, Ca2+ ions, an allosteric activator of calcium uptake in rat liver mitochondria. *Arch Biochem Biophys* **251**, 525-535 (1986).

18. A. Vinogradov, A. Scarpa, The initial velocities of calcium uptake by rat liver mitochondria. *J Biol Chem* **248**, 5527-5531 (1973).

19. J. M. Baughman *et al.*, Integrative genomics identifies MCU as an essential component of the mitochondrial calcium uniporter. *Nature* **476**, 341-345 (2011).

20. D. De Stefani, A. Raffaello, E. Teardo, I. Szabo, R. Rizzuto, A forty-kilodalton protein of the inner membrane is the mitochondrial calcium uniporter. *Nature* **476**, 336-340 (2011).

21. Y. Sancak *et al.*, EMRE is an essential component of the mitochondrial calcium uniporter complex. *Science* **342**, 1379-1382 (2013).

22. F. Perocchi *et al.*, MICU1 encodes a mitochondrial EF hand protein required for Ca(2+) uptake. *Nature* **467**, 291-296 (2010).

23. M. Plovanich *et al.*, MICU2, a paralog of MICU1, resides within the mitochondrial uniporter complex to regulate calcium handling. *PLoS One* **8**, e55785 (2013).

24. K. J. Kamer, V. K. Mootha, MICU1 and MICU2 play nonredundant roles in the regulation of the mitochondrial calcium uniporter. *EMBO Rep* **15**, 299-307 (2014).

25. M. Patron *et al.*, MICU1 and MICU2 finely tune the mitochondrial Ca2+ uniporter by exerting opposite effects on MCU activity. *Mol Cell* **53**, 726-737 (2014).

26. M. F. Tsai *et al.*, Dual functions of a small regulatory subunit in the mitochondrial calcium uniporter complex. *eLife* **5**, (2016).

27. M. Patron, V. Granatiero, J. Espino, R. Rizzuto, D. De Stefani, MICU3 is a tissue-specific enhancer of mitochondrial calcium uptake. *Cell Death Differ* **26**, 179-195 (2019).

28. K. Mallilankaraman *et al.*, MICU1 is an essential gatekeeper for MCU-mediated mitochondrial Ca(2+) uptake that regulates cell survival. *Cell* **151**, 630-644 (2012).

29. G. Csordas *et al.*, MICU1 controls both the threshold and cooperative activation of the mitochondrial Ca(2)(+) uniporter. *Cell Metab* **17**, 976-987 (2013).

30. C. V. Logan *et al.*, Loss-of-function mutations in MICU1 cause a brain and muscle disorder linked to primary alterations in mitochondrial calcium signaling. *Nat Genet* **46**, 188-193 (2014).

31. S. de la Fuente, J. Matesanz-Isabel, R. I. Fonteriz, M. Montero, J. Alvarez, Dynamics of mitochondrial Ca2+ uptake in MICU1-knockdown cells. *Biochem J* **458**, 33-40 (2014).

558 32. J. C. Liu *et al.*, MICU1 Serves as a Molecular Gatekeeper to Prevent In Vivo Mitochondrial Calcium
559 Overload. *Cell Rep* **16**, 1561-1573 (2016).
560
561 33. C. B. Phillips, C. W. Tsai, M. F. Tsai, The conserved aspartate ring of MCU mediates MICU1 binding
562 and regulation in the mitochondrial calcium uniporter complex. *eLife* **8**, (2019).
563
564 34. M. Paillard *et al.*, MICU1 Interacts with the D-Ring of the MCU Pore to Control Its Ca(2+) Flux and
565 Sensitivity to Ru360. *Mol Cell* **72**, 778-785 e773 (2018).
566
567 35. J. Matesanz-Isabel *et al.*, Functional roles of MICU1 and MICU2 in mitochondrial Ca(2+) uptake.
568 *Biochim Biophys Acta* **1858**, 1110-1117 (2016).
569
570 36. A. N. Antony *et al.*, MICU1 regulation of mitochondrial Ca(2+) uptake dictates survival and tissue
571 regeneration. *Nat Commun* **7**, 10955 (2016).
572
573 37. D. Lewis-Smith *et al.*, Homozygous deletion in MICU1 presenting with fatigue and lethargy in
574 childhood. *Neurol Genet* **2**, e59 (2016).
575
576 38. S. Musa *et al.*, A Middle Eastern Founder Mutation Expands the Genotypic and Phenotypic
577 Spectrum of Mitochondrial MICU1 Deficiency: A Report of 13 Patients. *JIMD Rep* **43**, 79-83 (2019).
578
579 39. G. Bhosale *et al.*, Pathological consequences of MICU1 mutations on mitochondrial calcium
580 signalling and bioenergetics. *Biochim Biophys Acta* **1864**, 1009-1017 (2017).
581
582 40. D. G. Nicholls, Mitochondria and calcium signaling. *Cell Calcium* **38**, 311-317 (2005).
583
584 41. V. Garg, Y. Y. Kirichok, Patch-Clamp Analysis of the Mitochondrial Calcium Uniporter. *Methods*
585 *Mol Biol* **1925**, 75-86 (2019).
586
587 42. K. J. Kamer *et al.*, MICU1 imparts the mitochondrial uniporter with the ability to discriminate
588 between Ca(2+) and Mn(2+). *Proc Natl Acad Sci U S A* **115**, E7960-E7969 (2018).
589
590 43. H. Vais *et al.*, EMRE Is a Matrix Ca(2+) Sensor that Governs Gatekeeping of the Mitochondrial
591 Ca(2+) Uniporter. *Cell Rep* **14**, 403-410 (2016).
592
593 44. N. E. Hoffman *et al.*, MICU1 motifs define mitochondrial calcium uniporter binding and activity.
594 *Cell Rep* **5**, 1576-1588 (2013).
595
596 45. N. Ishihara *et al.*, Mitochondrial fission factor Drp1 is essential for embryonic development and
597 synapse formation in mice. *Nat Cell Biol* **11**, 958-966 (2009).
598
599 46. J. Suzuki *et al.*, Imaging intraorganellar Ca2+ at subcellular resolution using CEPIA. *Nat Commun*
600 **5**, 4153 (2014).
601
602 47. X. Pan *et al.*, The physiological role of mitochondrial calcium revealed by mice lacking the
603 mitochondrial calcium uniporter. *Nat Cell Biol* **15**, 1464-1472 (2013).
604

605 48. E. Kovacs-Bogdan *et al.*, Reconstitution of the mitochondrial calcium uniporter in yeast. *Proc Natl*
606 *Acad Sci U S A* **111**, 8985-8990 (2014).
607
608 49. A. Raffaello *et al.*, The mitochondrial calcium uniporter is a multimer that can include a dominant-
609 negative pore-forming subunit. *Embo J* **32**, 2362-2376 (2013).
610
611 50. K. J. Kamer, Z. Grabarek, V. K. Mootha, High-affinity cooperative Ca(2+) binding by MICU1-MICU2
612 serves as an on-off switch for the uniporter. *EMBO Rep* **18**, 1397-1411 (2017).
613
614 51. P. Bernardi, A. Angrilli, G. F. Azzone, A gated pathway for electrophoretic Na+ fluxes in rat liver
615 mitochondria. Regulation by surface Mg2+. *Eur J Biochem* **188**, 91-97 (1990).
616
617 52. J. P. Wehrle, M. Jurkowitz, K. M. Scott, G. P. Brierley, Mg2+ and the permeability of heart
618 mitochondria to monovalent cations. *Arch Biochem Biophys* **174**, 313-323 (1976).
619
620 53. C. Petrungaro *et al.*, The Ca(2+)-Dependent Release of the Mia40-Induced MICU1-MICU2 Dimer
621 from MCU Regulates Mitochondrial Ca(2+) Uptake. *Cell Metab* **22**, 721-733 (2015).
622
623 54. Y. Xing *et al.*, Dimerization of MICU Proteins Controls Ca(2+) Influx through the Mitochondrial
624 Ca(2+) Uniporter. *Cell Rep* **26**, 1203-1212 e1204 (2019).
625
626 55. R. Rizzuto *et al.*, Close contacts with the endoplasmic reticulum as determinants of mitochondrial
627 Ca2+ responses. *Science* **280**, 1763-1766 (1998).
628
629 56. E. Neher, Vesicle pools and Ca2+ microdomains: new tools for understanding their roles in
630 neurotransmitter release. *Neuron* **20**, 389-399 (1998).
631
632 57. G. C. Faas, S. Raghavachari, J. E. Lisman, I. Mody, Calmodulin as a direct detector of Ca2+ signals.
633 *Nat Neurosci* **14**, 301-304 (2011).
634
635 58. P. Bernardi, V. Petronilli, The permeability transition pore as a mitochondrial calcium release
636 channel: a critical appraisal. *J Bioenerg Biomembr* **28**, 131-138 (1996).
637
638 59. F. Ichas, L. S. Jouaville, J. P. Mazat, Mitochondria are excitable organelles capable of generating
639 and conveying electrical and calcium signals. *Cell* **89**, 1145-1153 (1997).
640
641 60. M. Montero, M. T. Alonso, A. Albillos, J. Garcia-Sancho, J. Alvarez, Mitochondrial Ca(2+)-induced
642 Ca(2+) release mediated by the Ca(2+) uniporter. *Mol Biol Cell* **12**, 63-71 (2001).
643
644 61. U. Igbavboa, D. R. Pfeiffer, Regulation of reverse uniport activity in mitochondria by
645 extramitochondrial divalent cations. Dependence on a soluble intermembrane space component.
646 *J Biol Chem* **266**, 4283-4287 (1991).
647
648 62. H. Vais *et al.*, EMRE Is a Matrix Ca(2+) Sensor that Governs Gatekeeping of the Mitochondrial
649 Ca(2+) Uniporter. *Cell reports* **14**, 403-410 (2016).
650

651 63. T. E. Gunter *et al.*, An analysis of the effects of Mn2+ on oxidative phosphorylation in liver, brain,
652 and heart mitochondria using state 3 oxidation rate assays. *Toxicol Appl Pharmacol* **249**, 65-75
653 (2010).
654
655 64. J. Wettmarshausen *et al.*, MICU1 Confers Protection from MCU-Dependent Manganese Toxicity.
656 *Cell Rep* **25**, 1425-1435 e1427 (2018).
657
658 65. B. Hille, *Ionic channels of excitable membranes*. (Sinauer Associates, Sunderland, Mass., ed. 2nd,
659 1992), pp. xiii, 607.
660
661 66. A. P. Wescott, J. P. Y. Kao, W. J. Lederer, L. Boyman, Voltage-energized calcium-sensitive ATP
662 production by mitochondria. *Nature Metabolism* **1**, 975-984 (2019).
663
664 67. M. S. Bertolini, M. A. Chiurillo, N. Lander, A. E. Vercesi, R. Docampo, MICU1 and MICU2 Play an
665 Essential Role in Mitochondrial Ca(2+) Uptake, Growth, and Infectivity of the Human Pathogen
666 Trypanosoma cruzi. *MBio* **10**, (2019).
667
668 68. R. Tufi *et al.*, Comprehensive Genetic Characterization of Mitochondrial Ca(2+) Uniporter
669 Components Reveals Their Different Physiological Requirements In Vivo. *Cell Rep* **27**, 1541-1550
670 e1545 (2019).
671
672 69. F. A. Ran *et al.*, Genome engineering using the CRISPR-Cas9 system. *Nat Protoc* **8**, 2281-2308
673 (2013).
674
675 70. G. Grynkiewicz, M. Poenie, R. Y. Tsien, A new generation of Ca2+ indicators with greatly improved
676 fluorescence properties. *J Biol Chem* **260**, 3440-3450 (1985).
677
678 71. D. A. Winter, *Biomechanics and motor control of human movement*. (Wiley, Hoboken, N.J., ed.
679 4th, 2009), pp. xiv, 370 pages.
680
681 72. D. D. Hall, Y. Wu, F. E. Domann, D. R. Spitz, M. E. Anderson, Mitochondrial calcium uniporter
682 activity is dispensable for MDA-MB-231 breast carcinoma cell survival. *PLoS One* **9**, e96866 (2014).
683
684 73. G. Bhosale *et al.*, Pathological consequences of MICU1 mutations on mitochondrial calcium
685 signalling and bioenergetics. *Biochim Biophys Acta Mol Cell Res* **1864**, 1009-1017 (2017).

686

ACKNOWLEDGEMENTS

We thank Drs. Katsuyoshi Mihara (Kyushu University, Japan) and David C. Chan (Caltech, USA) for sending us *Drp1*$^{-/-}$ MEFs, and Dr. Toren Finkel (University of Pittsburgh, USA) for sending the MEFs with intact Drp1 (*WT* and *MICU1*$^{-/-}$ MEFs). We thank the Nikon Microscopy Core (DeLaine Larsen, Kari Herrington) and Lab for Cell Analysis (Sarah Elms) at UCSF for help with use of microscopy and FACS equipment. We thank all members of the Y.K. lab for helpful discussions; **Funding:** This work was supported by American Heart Association Scientist Development Grant 17SDG33660926 (V.G.) and NIH grant 5R01GM107710 (Y.K.); **Author contributions:** V.G. and Y.K. conceived the project and designed all experiments. V.G. performed all experiments. V.G. and T.U. performed Western blot experiments. J.S. consulted on Ca^{2+} imaging experiments. I.P. helped with the analysis of Ca^{2+} imaging experiments. L.S.M. consulted on single-channel analysis using QuB. V.G and Y.K. discussed the results and wrote the manuscript. All authors commented on the manuscript; **Competing interests:** Authors declare no competing interests; **Data and materials availability:** All data is available in the main text or the supplementary materials. Further information and requests for reagents may be directed to the lead contact Yuriy Kirichok (yuriy.kirichok@ucsf.edu).

SUPPLEMENTARY MATERIALS

Materials and Methods

Figure S1 – S10

Tables S1 – S2

References

FIGURE LEGENDS

Fig. 1. MCU-mediated I_{Ca} in *WT* and knockouts of MCU complex subunits. (**A**) Inward I_{Ca} elicited by a voltage ramp in *WT*, *MCU*$^{-/-}$ and *EMRE*$^{-/-}$ mitoplasts exposed to $[Ca^{2+}]_{cyto}$ of 30 µM, 100 µM and 1 mM. In *WT*, also note an outward Na^+ current via MCU at positive voltages in Ca^{2+}-free bath solution (Control). Voltage protocol is indicated on the top. (**B**) I_{Ca} is rescued by the recombinant expression of MCU and EMRE in their respective knockout cell lines. (**C**) I_{Ca} density measured at -160 mV at different $[Ca^{2+}]_{cyto}$ in indicated cell lines. (n = 4 to 5 each) Mean ± SEM. (**D**) Inward I_{Ca} in *WT*, *MICU1*$^{-/-}$, *MICU2*$^{-/-}$ and *MICU3*$^{-/-}$ mitoplasts exposed to 10 µM, 100 µM and 1 mM $[Ca^{2+}]_{cyto}$.. (**E**) I_{Ca} amplitudes measured at -160 mV in mitoplasts at $[Ca^{2+}]_{cyto}$ of 10 µM, 100 µM and 1 mM (*upper*), as well as 5 mM and 25 mM (*lower*). (n = 8 to 17) Mean ± SEM; one-way ANOVA with post-hoc Tuckey test. ***p< 0.01; ****p< 0.001.

Fig. 2. MICU1 is a Ca^{2+}-dependent MCU potentiator. (**A**) Representative I_{Na} in *WT*, *MCU*$^{-/-}$ and *EMRE*$^{-/-}$ mitoplasts at 110 mM $[Na^+]_{cyto}$. (**B**) I_{Na} amplitudes measured at -80 mV in *WT* (n = 20), *MCU*$^{-/-}$ (n = 3) and *EMRE*$^{-/-}$ (n = 3) mitoplasts. (**C**) Representative I_{Ca} (*blue*) and I_{Na} (*red*) recorded from the same *WT* and *MICU1*$^{-/-}$ mitoplasts exposed to 1 mM $[Ca^{2+}]_{cyto}$ or 110 mM $[Na^+]_{cyto}$. (**D** to **F**), Amplitudes of I_{Na} (D) and I_{Ca} (E), and the I_{Ca}/I_{Na} ratio in the same mitoplast (F) in *WT* (n = 27) and *MICU1*$^{-/-}$ (n = 18). Current were measured at -80 mV. Mean ± SEM; unpaired t-test, two-tailed. ****p< 0.001. (**G**) Inward I_{Na} recorded in the absence of cytosolic Ca^{2+} (*blue*) and subsequently at 2 nM $[Ca^{2+}]_{cyto}$ (*red*) in *WT* (*left*) and *MICU1*$^{-/-}$ (*right*) mitoplasts exposed to 110 mM $[Na^+]_{cyto}$. (**H**) Inhibition of I_{Na} by 2 nM $[Ca^{2+}]_{cyto}$ in *WT* and *MICU1*$^{-/-}$. Mean ± SEM; unpaired t-test, two-tailed (n = 4 each).

Fig. 3. Effects of MICU proteins and their EF hands on the amplitude, kinetics and rectification of I_{Ca}. (**A**) Western blots showing overexpression of MICU proteins or MICU proteins with non-functional EF hands (mut-EF-MICU) in their respective knockout background (*left*, *MICU1*$^{-/-}$; *middle*, *MICU2*$^{-/-}$ and; *right*, *MICU3*$^{-/-}$). (**B** to **D**) *Upper panels:* I_{Ca} in *MICU1*$^{-/-}$ (B), *MICU2*$^{-/-}$ (C) and *MICU3*$^{-/-}$ (D) before and after overexpression of a corresponding MICU subunit or its EF hand mutant, as compared to *WT*. To simplify comparison, representative I_{Ca} traces recorded from the mitoplasts of different backgrounds in 1 mM $[Ca^{2+}]_{cyto}$ are shown together in a single panel. *Lower panels:* quantification of I_{Ca} amplitudes from the upper panel at -160 mV. The same *WT* and knockout data were used as in Fig. 1e. Mean ± SEM; one-way ANOVA with post-hoc Tuckey test (n = 7 to 26). *p< 0.05; **p< 0.01; ***p< 0.001. (**E**) *Left panel*: I_{Ca} measured at a holding voltage of -100 mV while $[Ca^{2+}]_{cyto}$ was rapidly (τ ~0.4 ms, see Methods) switched from virtual zero to 1 mM and then back to virtual zero in *WT* (*grey*) and *MICU1*$^{-/-}$ (*red*) mitoplasts. *Right panel*, I_{Ca} kinetics within ~10 ms after the fast $[Ca^{2+}]_{cyto}$ elevation and subsequent decrease in *WT* (*grey*) and *MICU1*$^{-/-}$ (*red*) mitoplasts from the left panel. I_{Ca} traces were normalized to the maximal amplitude to facilitate comparison of kinetics in *WT* and *MICU1*$^{-/-}$. (**F**) *Left*: I_{Ca} activation time constant (τ_a) in *WT* and *MICU1*$^{-/-}$; *Right*: I_{Ca} deactivation time constant (τ_d) in *WT* and *MICU1*$^{-/-}$. Mean ± SEM (n = 3, each). (**G**) I_{Ca} at $[Ca^{2+}]_{mito}$ = 2 mM and indicated $[Ca^{2+}]_{cyto}$ in *WT* and *MICU1*$^{-/-}$. Arrows point out where the amplitude of outward I_{Ca} was measured. Bar-graph shows the amplitude of outward I_{Ca} measured at +80 mV. n = 3, each $[Ca^{2+}]_{cyto}$.

Fig. 4. Open probability of the MCU channel is decreased in *MICU1*$^{-/-}$. (**A** and **B**) MCU single-channel currents (i_{Ca}) from inside-out IMM patches in *WT* (A) and *MICU1*$^{-/-}$ (B) recorded at indicated potentials in symmetrical 105 mM Ca^{2+}, and low-pass filtered at 0.3 kHz for display purposes. Arrows indicate closed state level, and downward deflections are the open state events. Multiple subconductance levels are clearly visible at -80 and -120 mV. (**C** to **E**) Single-channel amplitudes (C), open probability (P_o) (D), and time-averaged unitary current (E) (see Methods) in *WT* and *MICU1*$^{-/-}$ at indicated potentials. Mean ± SEM; unpaired t-test, two-tailed; n = 5–6, each. *p< 0.05; **p< 0.01.

Fig. 5. I_{Mn} is reduced in *MICU1*$^{-/-}$ to the similar extent as I_{Ca}. (**A** to **C**) Representative inward I_{Mn} in *WT* (A), *MCU*$^{-/-}$ (B) and *EMRE*$^{-/-}$ (C) mitoplasts at 5 mM $[Mn^{2+}]_{cyto}$. (**D**) I_{Mn} measured at -160 mV from *WT* (n = 6), *MCU*$^{-/-}$ (n = 5) and *EMRE*$^{-/-}$ (n = 3) mitoplasts. Mean ± SEM. (**E**) I_{MCU} amplitudes at 5 mM $[Ca^{2+}]_{cyto}$ and 5 mM $[Mn^{2+}]_{cyto}$ in *WT* mitoplasts. Currents were measured at -160 mV. Mean ± SEM; unpaired t-test, two-tailed; n = 6–14; ***p< 0.001. (**F**) Representative I_{Ca} (*blue*, $[Ca^{2+}]_{cyto}$=1 mM), I_{Mn} (*green*, $[Mn^{2+}]_{cyto}$=5 mM) and inhibition of I_{Ca} by Mn^{2+} (*red*, $[Ca^{2+}]_{cyto}$=1 mM and $[Mn^{2+}]_{cyto}$=1 mM) in *WT* and *MICU1*$^{-/-}$ mitoplasts. (**G** to **J**) I_{Mn} (G), I_{Ca} (H), I_{Mn}/I_{Ca} ratio (I, measured in the same mitoplasts), and inhibition of I_{Ca} by 1 mM $[Mn^{2+}]_{cyto}$ (J) in *WT* (n = 3–6) and *MICU1*$^{-/-}$ (n = 5–11). Mean ± SEM; unpaired t-test, two-tailed. **p< 0.01; ***p< 0.001.

Fig. 6. Gating models of the MCU complex. (**A**) Current model of the MCU complex gating and the role of MICU subunits. The MCU complex has two states: MICU-occluded and open. At

low $[Ca^{2+}]_{cyto}$, MICU subunits occlude the MCU pore and inhibit Ca^{2+} influx. As $[Ca^{2+}]_{cyto}$ is increased, Ca^{2+} binds to the EF hands of MICU subunits, the MICU-mediated occlusion is relieved, and the MCU pore is open. (**B**) New model of the MCU complex gating and the role of MICU subunits. The MCU complex is a constitutively active channel. The level of the MCU activity is determined by spontaneous transitions between the open and closed states and the equilibrium between them. At low $[Ca^{2+}]_{cyto}$, this equilibrium is such that the probability of the open and closed states are comparable. As $[Ca^{2+}]_{cyto}$ is increased and Ca^{2+} binds to the EF hands of MICU subunits, MICUs strongly shift the equilibrium to the open state, which leads to a significant increase in the probability of the open state (*Po*) and a robust increase in the MCU activity.

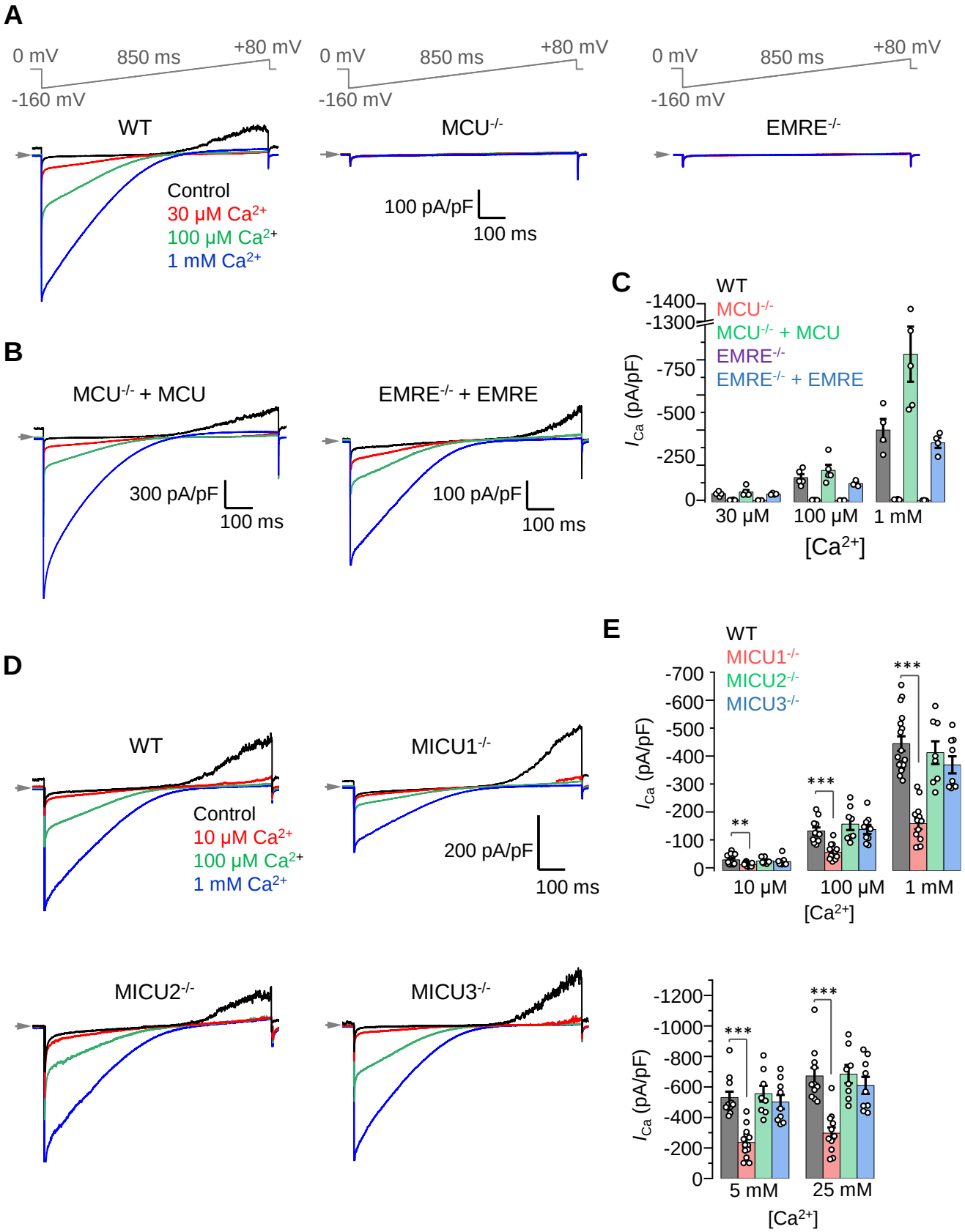
A
0 mV
850 ms
+80 mV
-160 mV
WT
Control
30 μM Ca2+
100 μM Ca2+
1 mM Ca2+
MCU-/-
100 pA/pF
100 ms
EMRE-/-
B
MCU-/- + MCU
300 pA/pF
100 ms
EMRE-/- + EMRE
100 pA/pF
100 ms
C
WT
MCU-/-
MCU-/- + MCU
EMRE-/-
EMRE-/- + EMRE
-1400
-1300
-750
-500
-250
0
ICa (pA/pF)
30 μM
100 μM
1 mM
[Ca2+]
D
WT
Control
10 μM Ca2+
100 μM Ca2+
1 mM Ca2+
MICU1-/-
200 pA/pF
100 ms
MICU2-/-
MICU3-/-
E
WT
MICU1-/-
MICU2-/-
MICU3-/-
-700
-600
-500
-400
-300
-200
-100
0
ICa (pA/pF)
**
***
***
10 μM
100 μM
1 mM
[Ca2+]
-1200
-1000
-800
-600
-400
-200
0
***
***
5 mM
25 mM
[Ca2+]

Fig. 1

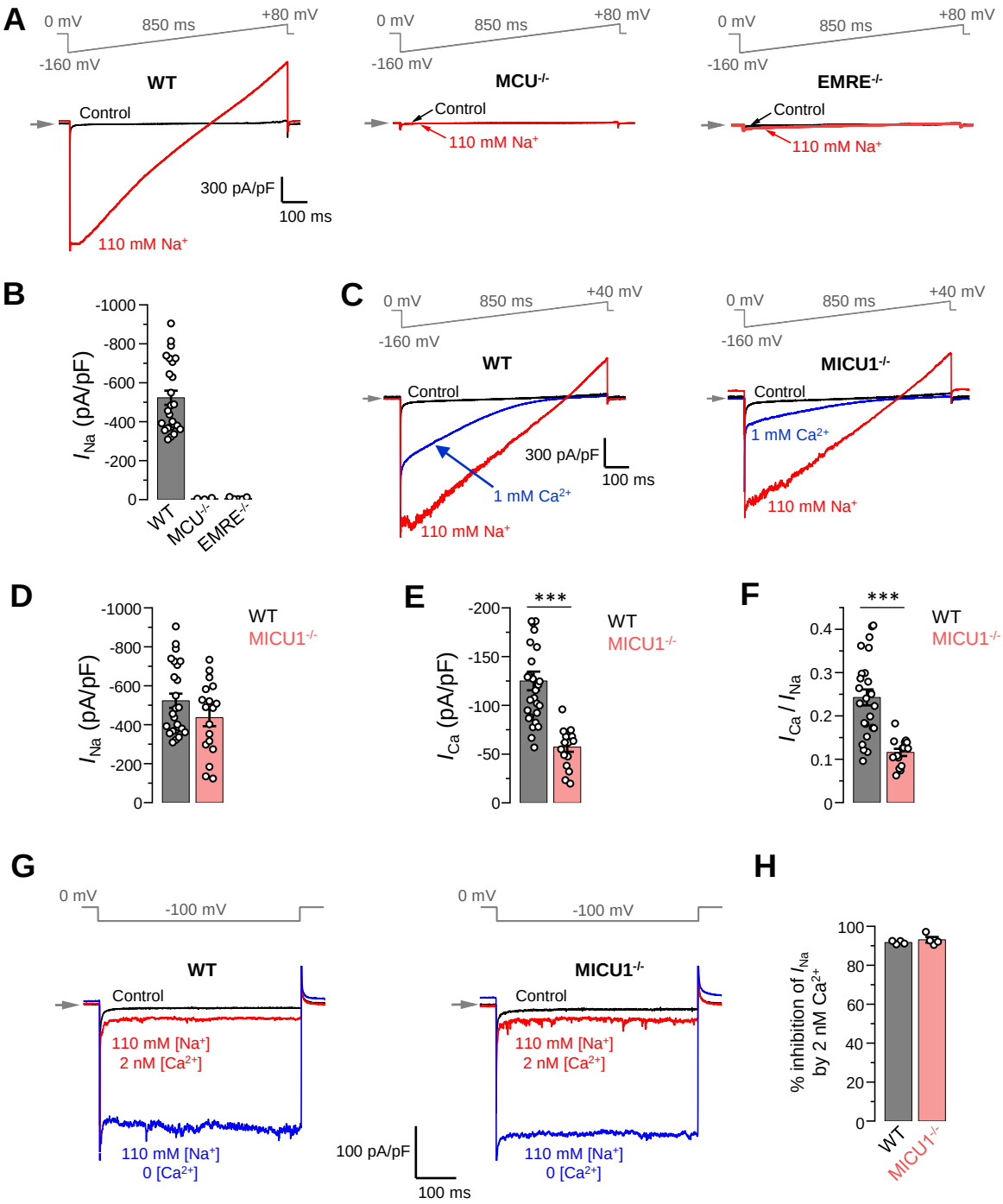
A
0 mV
850 ms
+80 mV
-160 mV
WT
Control
300 pA/pF
100 ms
110 mM Na+
MCU-/-
110 mM Na+
EMRE-/-
B
-1000
-800
-600
-400
-200
0
INa (pA/pF)
WT
MCU-/-
EMRE-/-
C
+40 mV
MICU1-/-
1 mM Ca2+
D
MICU1-/-
E
***
ICa (pA/pF)
F
ICa / INa
G
-100 mV
110 mM [Na+]
2 nM [Ca2+]
0 [Ca2+]
100 pA/pF
H
% inhibition of INa by 2 nM Ca2+

Fig. 2

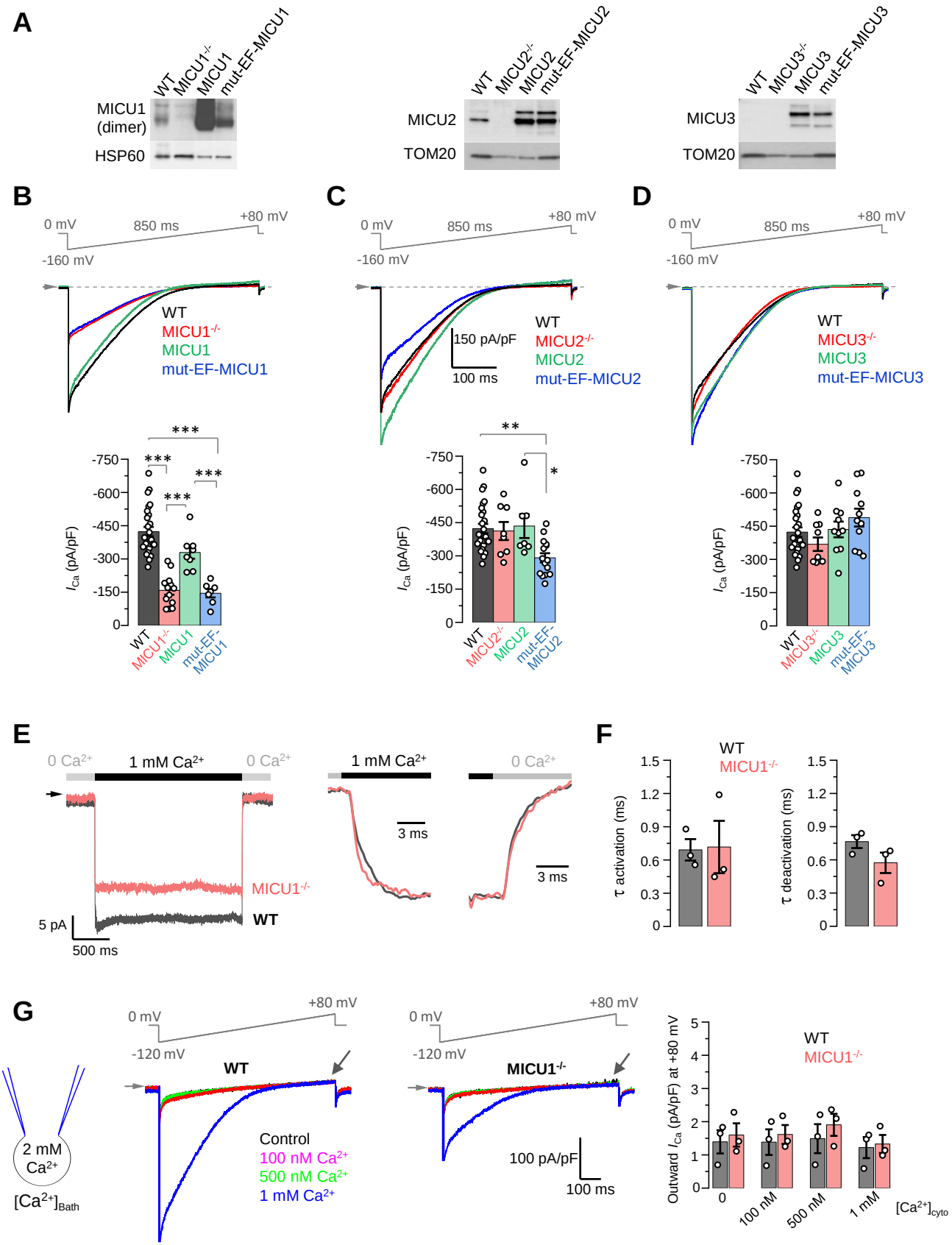
A
WT
MICU1-/-
MICU1
mut-EF-MICU1
MICU1 (dimer)
HSP60
WT
MICU2-/-
MICU2
mut-EF-MICU2
MICU2
TOM20
WT
MICU3-/-
MICU3
mut-EF-MICU3
MICU3
TOM20
B
0 mV
850 ms
+80 mV
-160 mV
WT
MICU1-/-
MICU1
mut-EF-MICU1
C
150 pA/pF
100 ms
WT
MICU2-/-
MICU2
mut-EF-MICU2
D
WT
MICU3-/-
MICU3
mut-EF-MICU3
ICa (pA/pF)
E
0 Ca2+
1 mM Ca2+
0 Ca2+
MICU1-/-
WT
5 pA
500 ms
3 ms
F
τ activation (ms)
τ deactivation (ms)
G
2 mM Ca2+
[Ca2+]Bath
-120 mV
Control
100 nM Ca2+
500 nM Ca2+
1 mM Ca2+
100 pA/pF
Outward ICa (pA/pF) at +80 mV
[Ca2+]cyto

Fig. 3

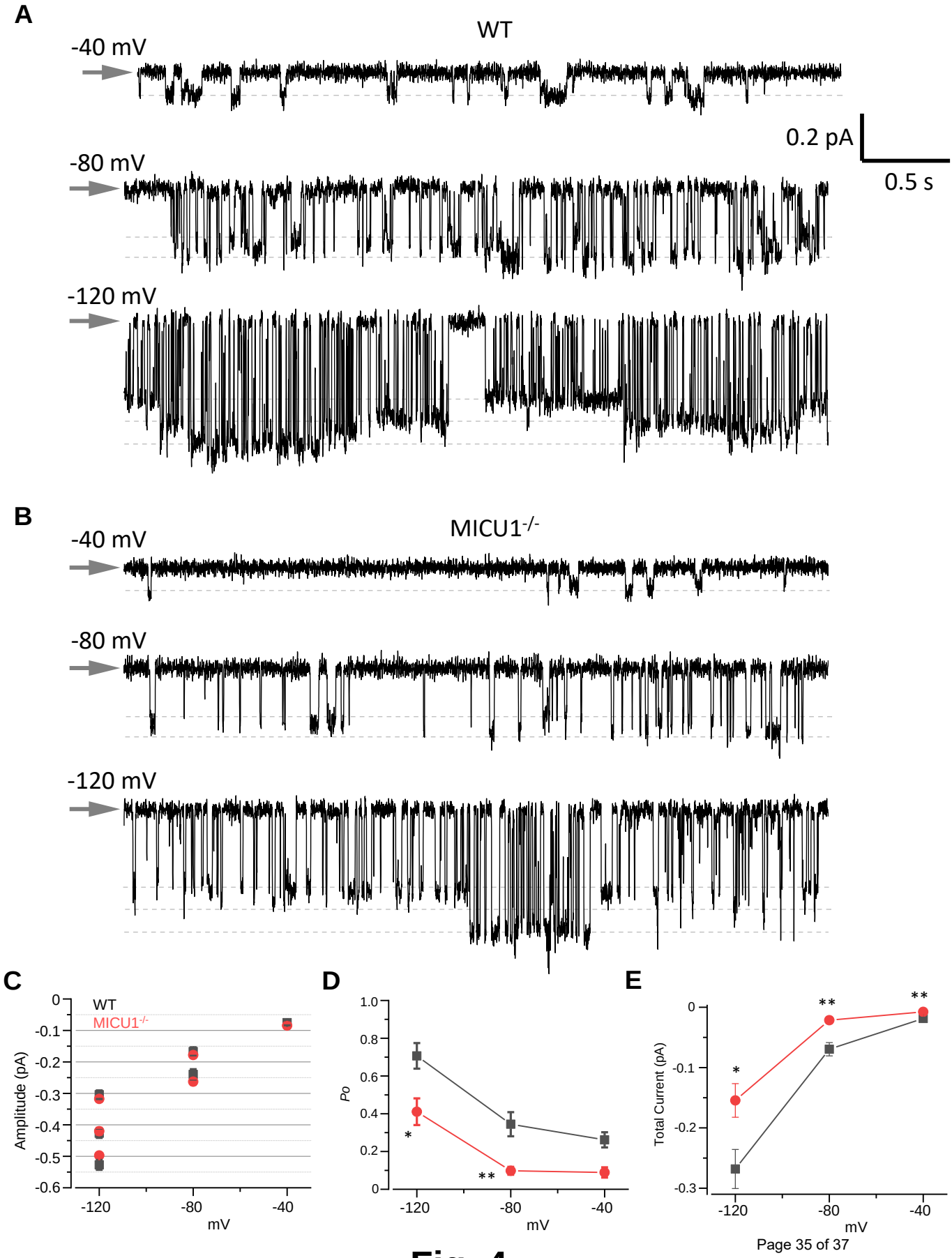
A
WT
-40 mV
-80 mV
-120 mV
0.2 pA
0.5 s
B
MICU1-/-
-40 mV
-80 mV
-120 mV
C
WT
MICU1-/-
Amplitude (pA)
0
-0.1
-0.2
-0.3
-0.4
-0.5
-0.6
-120
-80
-40
mV
D
Po
1.0
0.8
0.6
0.4
0.2
0
*
**
-120
-80
-40
mV
E
Total Current (pA)
0
-0.1
-0.2
-0.3
*
**
**
-120
-80
-40
mV

Fig. 4

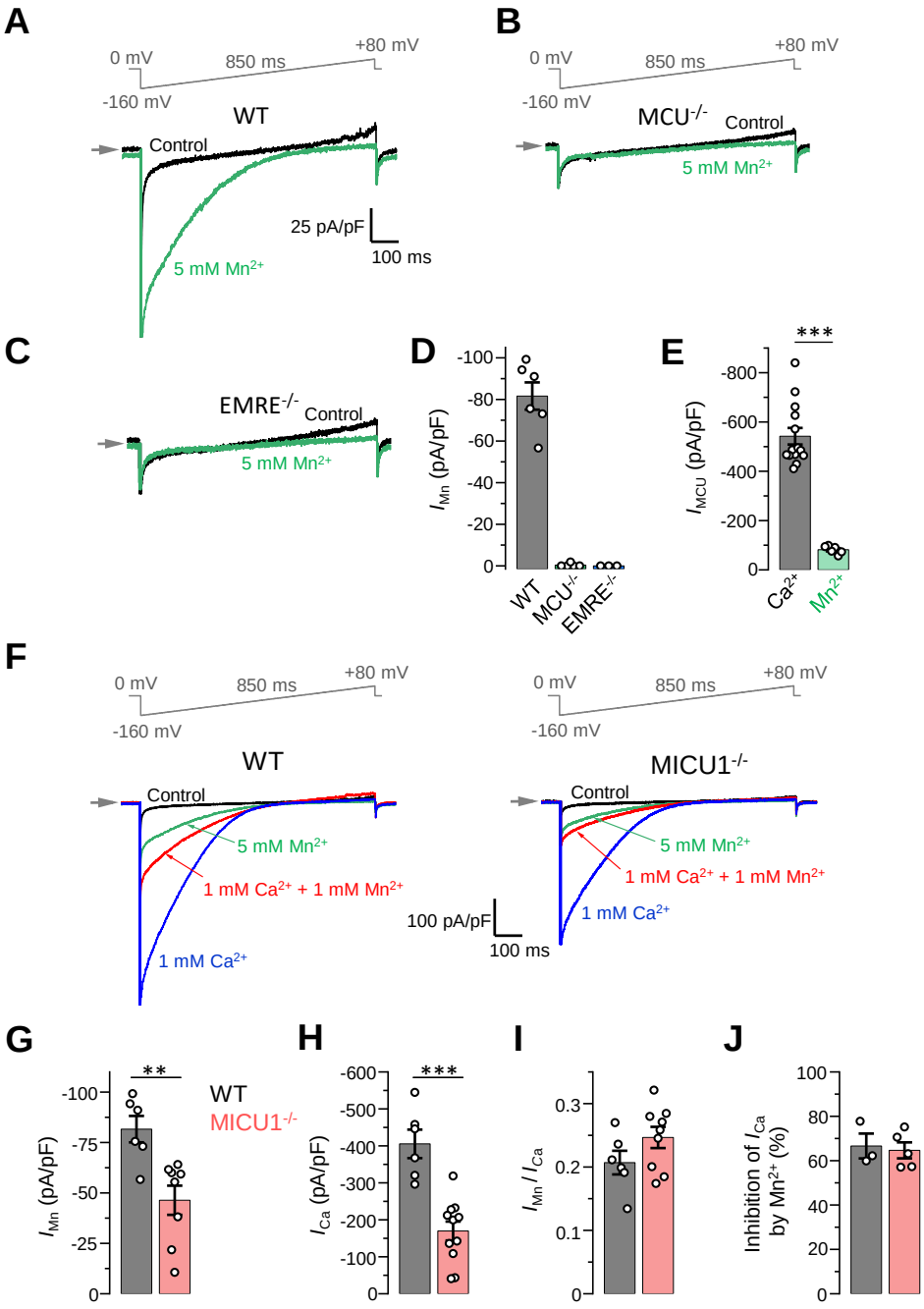
A
0 mV
850 ms
+80 mV
-160 mV
WT
Control
5 mM Mn2+
25 pA/pF
100 ms
B
MCU-/-
Control
5 mM Mn2+
C
EMRE-/-
Control
5 mM Mn2+
D
IMn (pA/pF)
WT
MCU-/-
EMRE-/-
E
***
IMCU (pA/pF)
Ca2+
Mn2+
F
WT
MICU1-/-
Control
5 mM Mn2+
1 mM Ca2+ + 1 mM Mn2+
1 mM Ca2+
100 pA/pF
100 ms
G
**
IMn (pA/pF)
WT
MICU1-/-
H
***
ICa (pA/pF)
I
IMn / ICa
J
Inhibition of ICa by Mn2+ (%)

Fig. 5

A

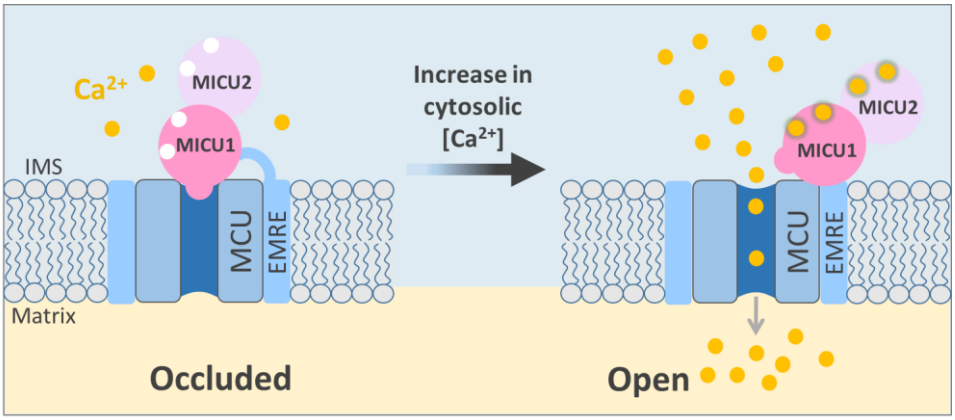

Old MCU Gating Model

B

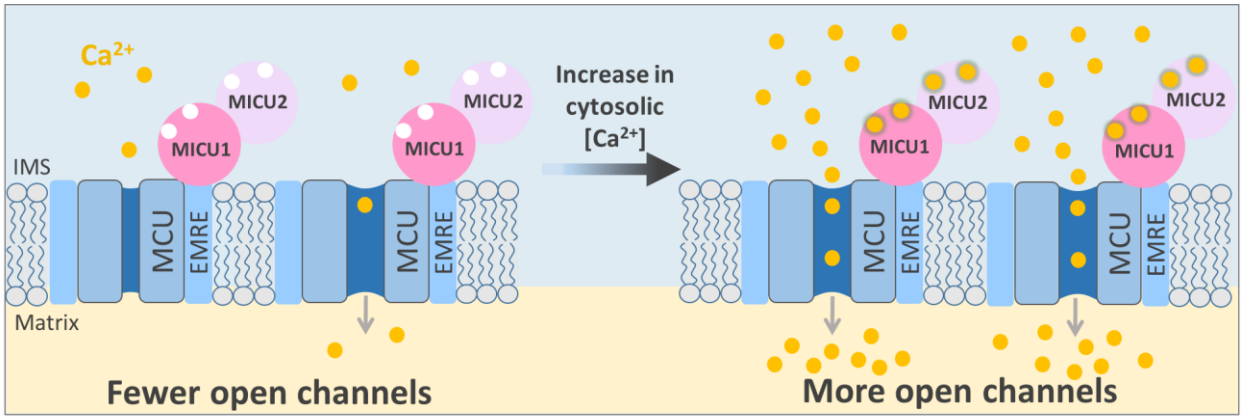

New MCU Gating Model

Fig. 6